

Asymmetric Optical Wavelength Switch Based on LCoS-SLM for Edge Node of Optical Access Network

Hsi-Hsir Chou  and Chia-Lun Chen 

Abstract—A novel design of optical wavelength switch, based on an asymmetric switching architecture for edge node implementation, is presented in this paper. Compared to previous research for optical core transport network applications, the proposed work has a unique aspect to build dynamic multicasting and spectral equalization, vital functionalities for optical wavelength switch in the edge of optical access networks. An optical wavelength switch was experimentally implemented and evaluated in a 4×16 switching architecture to demonstrate the concept. This dynamic multicasting and spectral equalization were achieved by utilizing liquid crystal on a silicon spatial light modulator (LCoS-SLM) device. An optimal design of computer-generated holograms (CGHs) through an improved GS algorithm was used to perform the beam steering and wavelength switching. A variety of wavelength switching scenarios has been experimentally evaluated. The measurement results showed an average insertion loss of around -12.5 dB, and the calculated crosstalks were all less than -28 dB. Its applications in digital data transmissions were evaluated to achieve a transmission speed larger than 2.5 Gbps. The eye diagram measurement results showed that most wavelength switching scenarios have nearly bit-error-free transmission. The scenario includes the multicasting with spectral equalization within the proposed asymmetrical switching architecture.

Index Terms—Optical wavelength switch, spatial light modulator, liquid crystal on silicon device.

I. INTRODUCTION

FAST deployment of wavelength division multiplexing (WDM) and dense WDM (DWDM) technologies in optical fiber transmission networks [1]–[4] have faced many severe challenges to implementing new reconfigurable edge node architectures for fiber network access. The next-generation of infrastructure for an optical access network requires many essential features for high-speed data transmission. In addition to the fundamental wavelengths, flexible bandwidth, and enhanced capacity, it is necessary to have low latency, low cost, and reconfigurable edge node architecture for maximum information throughput. Network resilience with good overall network reliability is also desired.

Manuscript received March 29, 2021; revised June 18, 2021; accepted June 23, 2021. Date of publication June 28, 2021; date of current version July 20, 2021. The work was supported by the Ministry of Science and Technology (MOST), Taiwan under Grants MOST 106-2221-E-011-011, MOST 107-2622-E-011-028-CC3, and MOST 107-2221-E-011-048 (add-on grant for international collaboration). (*Corresponding author: Hsi-Hsir Chou.*)

The authors are with the Department of Electronic and Computer Engineering, National Taiwan University of Science and Technology, Taipei 106, Taiwan (e-mail: hsi-hsir.chou@trinity.cantab.net; m10402340@mail.ntust.edu.tw).

Digital Object Identifier 10.1109/JPHOT.2021.3092734

One of the potential solutions to produce these features is to implement a new optical wavelength switch on the reconfigurable optical add-drop multiplexer (ROADM), acting as an edge node (i.e., the edge ROADM) for interfacing with the optical access network [5]. Several technologies, including thermo-optic waveguide switches [6], 1D/2D MEMS [7]–[8], and polarization-modulated liquid crystal (LC) switches [9], have been developed for ROADM applications in an optical core transport network. Liquid Crystal on Silicon (LCoS) based optical wavelength switches were considered the most key-enabling technology in future optical networks [10]–[11]. Moreover, hologram beam steering switches based on LCoS spatial light modulator (SLM) have been reported as a promising optical switch technology for edge node application [12]. However, the previously demonstrated optical switches based on LCoS devices, even supporting multicasting, were limited to a $1 \times N$ switching architecture [13]–[15]. Although an $M \times N$ optical wavelength switch based on LCoS-SLM has been reported [16], the evaluation works were only performed through a symmetrical switching architecture. Moreover, only a minimal switching dimension, i.e., 4×4 , has been used.

Optical wavelength switches based on a symmetric switching architecture are very suitable for ROADM applications in an optical core transport network. They will increase the degrees of freedom in the ROADM because the input/output links in optical core transport networks are usually configured symmetrically. However, for the implementation of an edge node between the optical core transport network and the optical fiber access network, an optical wavelength switch based on asymmetrical switching architecture would help distribute the high-speed data rate to many clients. Although a new optical wavelength switch based on an asymmetric 8×24 switching architecture has recently been presented and seems to be commercially available [17], it was based on the utilization of MEMS and LCoS technologies for core transport network application. Moreover, the performance and characteristics of multicasting and spectral equalization have not been thoroughly investigated. These are important for an optical edge node in the optical fiber access network.

In this paper, a reconfigurable optical wavelength switch utilizing the LCoS-SLM device in an asymmetric wavelength switching architecture, as illustrated in Fig. 1, is presented. It is the first time for edge node (i.e., e-ROADM) implementation to the best of our knowledge. Dynamic multicasting (up to 16

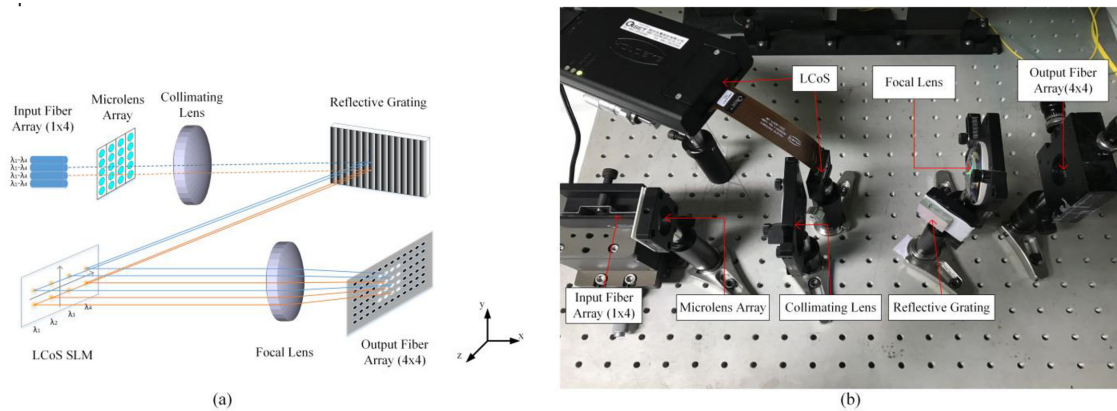


Fig. 1. Optical wavelength switch based on 4×16 asymmetrical switching configuration (a) System architecture, (b) Experimental setup.

ports simultaneously) and spectral equalization, which are the vital functionalities required for the optical transport network to interface with the optical fiber access network, were implemented through the design of computer-generated-holograms (CGHs). The design of these CGHs was based on an optimal procedure of the Gerchberg-Saxton (GS) algorithm [18], [19]. An asymmetric optical wavelength switch system in a 4×16 switching architecture was experimentally implemented for performance evaluation. Digital signal transmission tests were conducted at a transmission speed beyond 2.5 Gbps successfully. Progressing from our previous works in [19]–[20], we further report the proposed optical wavelength switch system’s design consideration. The system performance evaluation, including system insertion loss, crosstalk, and data transmission tests in the multicasting scenarios, are analyzed. The proposed optical wavelength switch system will offer a direct approach to efficiently implementing a reliable edge node architecture for an optical fiber access network.

II. EXPERIMENTAL SYSTEM ARCHITECTURE

A. System Architecture

The proposed optical wavelength switch system based on an asymmetric switching architecture in a 4×16 switching configuration is illustrated in Fig. 1. All optical elements were stabilized in sequential order in a compact “Z” configuration on an optical breadboard through optomechanics, which has also been utilized to control and align the relative positions for experimental setup and measurement. The proposed work’s vital component is the LCoS-SLM device, which was purchased from HOLOEYE Photonics AG and is composed of an array of 1920×1080 pixels. Given that 24 pixels along the dispersion axis were allocated to each 50 GHz channel, the whole C-band with 80 such channels will be covered. Note that 21×21 pixels can be used to steer the beam to 4 positions [21]. Moreover, a higher resolution LCoS-SLM device, i.e., Jasper JD2704 [22], with 4096×2400 pixels can also be commercially purchased and applied in the proposed work. The pixel pitch of the used LCoS-SLM device is $8.0 \mu\text{m}$, providing an active area of “0.7” in the diagonal size with an aspect ratio of 16:9. The filling

factor is 0.93. All pixels are controlled by uploading predesigned hologram profiles and applying external voltages of 256 levels between 0 and 10 V to the liquid crystal using the computer’s DVI signals. Therefore, the LCoS-SLM device can resolve 256 discrete modulation levels at a maximum phase depth of 2π at 1550 nm. Except for the phase-only LCoS-SLM device, the rest of the optical wavelength switch system comprises four parts: the input & output fiber plane (array), lens system, and a fixed period of phase grating element (Newport, 1100 lines/mm). The fiber plane is composed of SMF-fiber-arrays (each fiber is spacing by 250 μm). The lens system includes a set of microlens (diameter: 12×12 mm, focal length: 0.42 mm, pitch: 250 μm , SUSS Micro-Optics), a collimating lens (diameter: 50.8 mm, focal length: 100 mm, Thorlabs) and a focal lens (diameter: 50.8 mm, focal length: 60 mm, Thorlabs). The switching system was designed to perform the optical wavelength switching between the input fiber plane and output fiber plane. Each incident wavelength from the input fiber can be arbitrarily switched/multicast to any/all optical fibers in the output fiber plane. The add function can be performed when the wavelengths are added to the input fiber and then are steered to the output fiber for external transmission. The drop function can be performed by steering the wavelengths from input fiber to the output fiber for local access. For the proof of concept, multiple wavelengths in C-band spacing by 100 GHz between 1550 nm and 1554.8 nm were multiplexed in each input fiber. The 3-dB modulation bandwidth of each wavelength is 9.6 GHz, which can easily achieve a data rate of over 10 Gbit/s using the OOK modulation scheme. It is also possible to achieve a data rate of over 20 Gbit/s if the PAM-4 modulation scheme is used according to Shannon’s theory [23]. The polarization of these multiplexed wavelengths was aligned parallel to the LC materials’ director to improve the phase modulation efficiency of the LCoS-SLM device as they are polarization-sensitive. Therefore, these incoming wavelengths, which were launched from the polarization-maintaining (PM) input fiber array, were collimated by a microlens array and a collimating lens before the incidence on a static grating component. Because the pixel pitch of the used LCoS-SLM device technology ($8.0 \mu\text{m}$) is not small enough to perform a targeted grating period for wavelength separation. The grating component’s fixed period and the LCoS-SLM

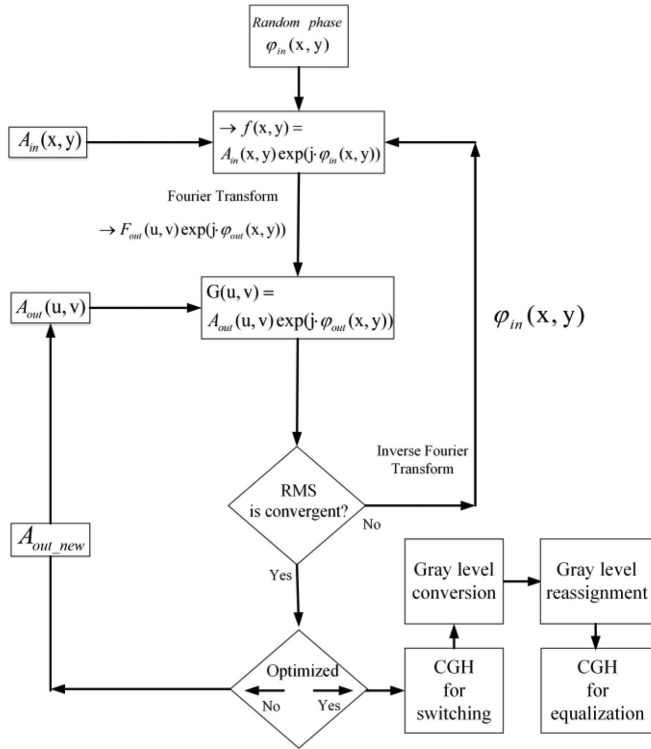


Fig. 2. Flow chart of an optimized GS algorithm.

device displaying dynamic CGHs were utilized to conduct each transmission wavelength's beam steering. The spatial separation of incident wavelengths on the LCoS-SLM device was angularly converted from the static grating component's diffraction. Each wavelength incident on the LCoS-SLM device was controlled independently by a sub-hologram, and the used hologram can also be further replaced by using different CGHs. These CGHs were generated from an optimal designing approach [19] based on a conventional GS algorithm (a Fourier-transform based iterative algorithm). The flow chart of the optimized GS algorithm is shown in Fig. 2.

As illustrated in Fig. 3(a), the LCoS-SLM device was divided into four sub-planes spacing by "a" pixels. It was designed to conduct beam steering for incident light transmitted from different input fiber. Therefore, each sub-plane can be used to upload reconfigurable CGHs simultaneously. The width of the designed hologram (sub-hologram), uploaded into each sub-plane of the LCoS-SLM device, was determined by the parameter "b." Note that in Fig. 3, each sub-hologram period is represented by the parameter "T," and the minimum spacing between two adjacent sub-holograms was determined by the parameter "c." Except for the beam steering angle limited by the hologram period ("T"), similar to "a," a smaller "b" and "c" should be used to raise the utilization efficiency of the LCoS-SLM device. To reduce the light loss from each received wavelength's fiber coupling, which was deflected from the LCoS-SLM device, a focal lens was used between the LCoS-SLM device and the output fiber plane.

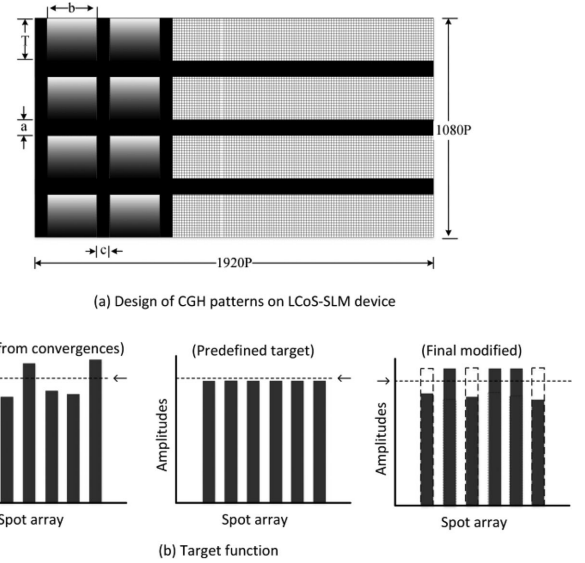


Fig. 3. Design of CGH patterns on LCoS-SLM device.

B. Switching Functionalities

For an edge node application, an optical wavelength switch's operational characteristic differs significantly from those used in a conventional optical transport network (i.e., core ROADM). These characteristic differences arise from the large distance variations of the optical access network in the edge node. Therefore, the functionalities of spectral equalization and multicasting should be included. In this research, multicasting and spectral power equalization are optimized by applying a GS algorithm [18]–[19] to the proposed optical wavelength switch system. Fig. 2 is the optimal procedure's flowchart based on the conventional GS algorithm utilized in our experimental research work. The operation principle is similar to the traditional GS algorithm since a phase $\varphi_{in}(x, y)$ distributed uniformly in the range $[0, 2\pi]$ is randomly chosen in the initial iterative procedure. A function $f(x, y)$ is defined as

$$f(x, y) = A_{in}(x, y) \exp[i\varphi_{in}(x, y)] \quad (1)$$

where $A_{in}(x, y)$ is the predefined spot amplitude distribution. The field distribution of output $F(u, v)$, which is a scaled Fourier transform of $f(x, y)$ is expressed as

$$F(u, v) = FT\{f(x, y)\} = F_{out} \exp[i\varphi_{out}(u, v)] \quad (2)$$

We replace the amplitude $F_{out}(u, v)$ by the predefined spot amplitude distribution in the Fourier plane, $A_{out}(u, v)$ and leave the phase φ_{out} unchanged as it is originated from (2). The following new function $G(u, v)$ is generated as

$$G(u, v) = A_{out}(u, v) \exp[i\varphi_{out}(u, v)] \quad (3)$$

We further conducted an inverse Fourier transform on $G(u, v)$ and used the phase obtained from (3) as the input phase $\varphi_{in}(x, y)$. The convergence criterion of the iterative procedures is determined by the RMS (root mean square) value, calculated by $RMS = \sqrt{\sum_{i=1}^n (P_t - P_i)^2}$, where n is the number of spots, P_t

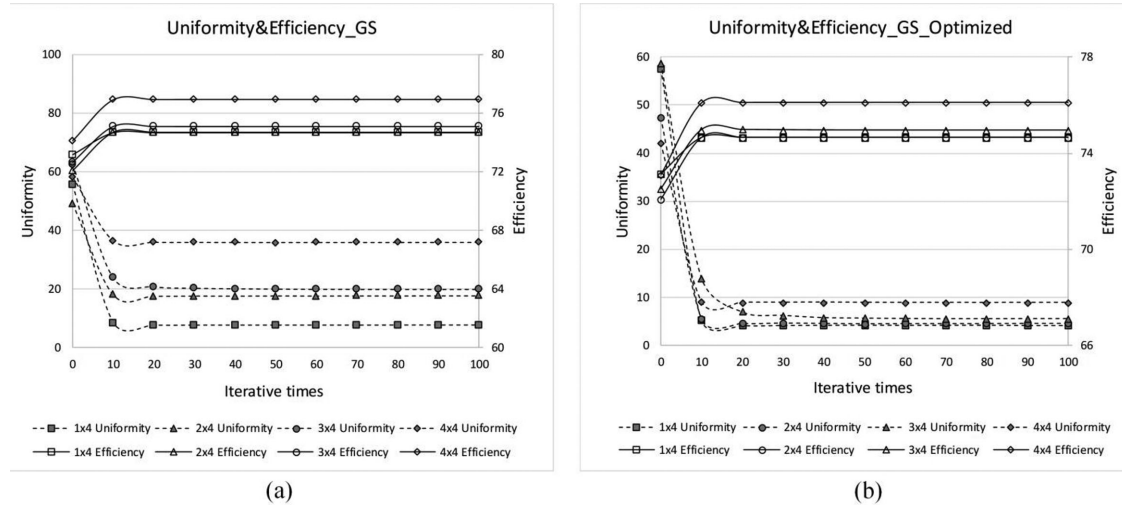


Fig. 4. Simulation performance of multispot configuration at far-field (a) GS algorithm (b) Optimal procedure based on GS algorithm.

is the predefined spot power and P_i is the power of the i_{th} spot. Since the stagnation effect characterizes the GS algorithm, it converges very fast with a speedy decrease of the RMS during the initial several iterative procedures. Still, no significant reduction in RMS will result from further iterations. Therefore, after the first initial several iterative procedures, the algorithm will be converged quickly and stagnate at local minima, resulting in a good efficiency and worst uniformity.

A balancing procedure was used in this research. In this procedure as shown in Fig. 3(b), the $A_{out}(u, v)$ obtained from the initial convergence of the first few iterative steps were further applied to modify the predefined spot amplitude distribution. A new distribution of spot amplitude (A_{out_new}) was formed for further GS iterative procedures. It was achieved by redefining the spot amplitude distribution to average the power values of spot amplitude distributions in the previous iterations as the new power value for the next iterations. Since the phase obtained of the prior convergence result of the GS algorithm has produced an excellent efficiency, this phase (not chosen randomly) combined with a new modified amplitude distribution was then used for further iterative procedures. After these iteration procedures, the uniformity of spot power distribution can be further optimized since the power amplitude distribution will be reallocated.

It is different from the previous research that focused on performance improvement at near-field through Fresnel approximation [19]. In our experimental works, the multispot configuration's performance at far-field was investigated through Fraunhofer approximation to better uniform spot power distribution. It will help enhance service reliability. The performance of dynamically spot array generation, which represents multicasting to 4, 8, 12, and 16 ports, respectively, was evaluated. Here the uniformity of spot power distributions is defined as $U = (P_{max} - P_{min}) / (P_{avg})$, where P_{max} is the maximum power of the spot, P_{min} is the minimum power of the spot and P_{avg} is the average spot power of all desired spots. The efficiency E is defined as $E = P_{total} / P_0$, where P_{total} is the power contained in all desired spots and P_0 is the total incident

power. From the simulation results shown in Fig. 4, for the scenarios of 4 ~ 16 spot array generation as the representative performance of multicasting to 4 ~ 16 ports, the generated spot array's power uniformity has been decreased from 38% to 10%. Compared with the original iterative procedure of the GS algorithm, the optimal procedure will provide an efficient approach to rapidly achieve an improved uniformity of spot power distributions while giving a good phase modulation efficiency as the conventional GS algorithm.

III. RESULTS & DISCUSSIONS

A. Light Loss & Crosstalk of the System

The light loss in the proposed optical wavelength switch system mostly resulted from the insertion losses of each used optical element, the diffractive grating component's efficiency in combination with the LCoS-SLM device, and the fiber coupling loss. A standard power meter (Thorlabs PM100D) was used in our experimental measurements, and the insertion losses of using different wavelengths were measured respectively. The results have shown that the lens system has an average insertion loss of 0.62 dB, which is resulted from the microlens array (0.14 dB), the collimating lens (0.25 dB), and the focal lens (0.23 dB). Although the static grating component has a theoretical efficiency higher than 90% [24], only about 67% was achieved from our measurements, and therefore an average light loss of 1.65 dB has resulted. The average insertion loss of the LCoS-SLM device was measured to be 2.49 dB under the setup of no CGH patterns uploaded. The LCoS-SLM device's efficiency was obtained based on the calculation as the +1st diffraction order power relative to the 0th diffraction order power when no CGH patterns were uploaded to the LCoS-SLM device. According to the experimental results, the phase modulation efficiency of the LCoS-SLM device was measured to be around 77.56%, and therefore an average light loss of 1.23 dB was measured. The light loss from fiber coupling in each fiber at the output plane of the switching system varies. Each incoming wavelength at the

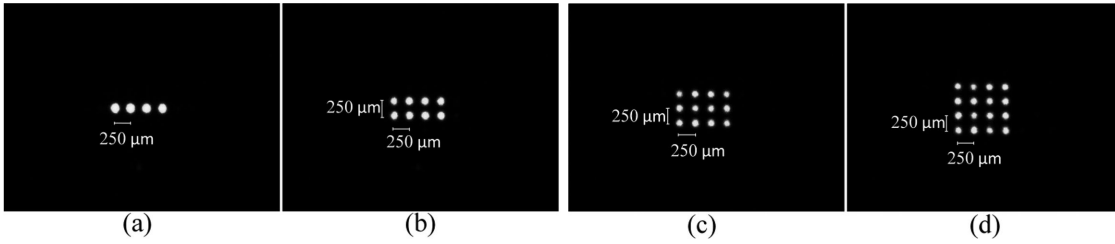


Fig. 5. Dynamic spot array patterns captured on the plane of output fiber array when multicasting to (a) 4 ports, (b) 8 ports, (c) 12 ports, (d) 16 ports.

TABLE I
WORSE CASE OF CROSSTALK IN THE SCENARIO OF MULTICASTING (dB)

1552.4nm	Port1	Port2	Port3	Port4
Crosstalk	-33.57	-36.42	-36.75	-35.30
1553.2nm	Port5	Port6	Port7	Port8
Crosstalk	-28.27	-32.06	-31.12	-29.41
1554nm	Port9	Port10	Port11	Port12
Crosstalk	-32.22	-34.70	-31.38	-34.51
1554.8nm	Port13	Port14	Port15	Port16
Crosstalk	-33.24	-36.63	-35.11	-32.44

output plane's targeted fiber port has a different physical offset, alignment error, and different diffraction efficiency. In the case of single-wavelength switching, i.e., switching the wavelength of 1554 nm from each input fiber port to any output fiber port, the average light loss caused by the low fiber coupling efficiency was around 6.5 dB, according to the measurement results. Therefore the average total system insertion loss is approximately 12.5 dB.

The proposed optical wavelength switch system's crosstalk is defined as the ratio of the optical power from all other input wavelengths to the optical power at the target output fiber from the desired input wavelength:

$$\text{Crosstalk} = 10 \log_{10} \left(\frac{P_u}{P_d} \right) \text{ (dB)} \quad (4)$$

where P_u is the optical power from all other unwanted input wavelengths, and P_d is the optical power from the desired input wavelength. The worst case of the system crosstalk that occurred in the multicasting scenario is shown in Table I. In this case, the wavelength of 1553.2 nm, multicasting to the output fiber port of 5 ~ 8 simultaneously, has the worse crosstalk ranging between -28~-32 dB. However, the crosstalk of all other wavelengths in the same scenario is less than -32 dB.

B. Uniformity of Multicasting

The intensity profiles of dynamically spot array generation at the plane of output fiber array, which is corresponding to the scenarios of multicasting to 4, 8, 12, 16 ports simultaneously, were captured by a CCD camera (Scintacor, Digital CamIR1550 463125) and are illustrated as in Fig. 5. The conventional knife-edge method [25] was used to conduct the proposed system architecture's performance measurement. The measurement results have shown that the spot uniformity of 7.8%, 10.3%, 17%,

and 18.4% was obtained, respectively, in multicasting scenarios to 4, 8, 12, and 16 ports simultaneously.

C. Multicasting With Power Equalization

The performance of power spectral equalization for each wavelength in multicasting scenarios was investigated. According to the measured results, the maximum optical power gap between each received optical wavelength is around 3.63 dB. This deviation can further decrease to 0.03 dB when power spectral equalization was used. The multicast switching scenario to demonstrate the performance is illustrated in Fig. 6. The performance of power spectral equalization is evaluated using 1550.8 nm wavelength delivered from input port 1. The measurement results show that the gap Δ of each output fiber port's received optical power with and without power equalization is around 0.01dB ~ 0.04dB. These gaps are almost identical in multicasting scenarios. The power spectral equalization was further examined using different wavelengths in the multicasting scenario. The results are shown in Fig. 7. In Fig. 7, the gap Δ of each wavelength's received optical power with/without power equalization is around 0.01dB. These experimental results have indicated that the application of power spectral equalization in multicast switching scenarios will not significantly influence spot power distributions' uniformity. The reasons are that the holograms used for power equalizations for each wavelength were reconfigured according to their original holograms that were generated for multicasting. Therefore, each wavelength can all reach the same targeted power after power equalization, even in the scenario of multicasting.

D. Digital Signal Transmission Tests

In the performance evaluation of the digital signal transmission test at a transmission speed beyond 2.5 Gbps, a pulse pattern generator (Keysight N4970A) was used to generate electrical signals based on a non-return-to-zero (NRZ) pseudo-random bit sequence (PRBS) of length $2^7 - 1$. These electrical signals have been used through external Lithium Niobate Electro-Optic Modulators (10 Gbit/s, Agere Systems Inc.) to modulate each optical wavelength delivered from tunable lasers (TLs) for the input fiber plane of the system and switched to output fiber plane. The eye diagrams of four different wavelengths delivered from input fiber port 1 ~ 4 respectively and multicasting to 16 output fiber ports of the switching system have been evaluated. The representative results are illustrated in Fig. 8, and 9, respectively, which have shown the measured eye diagrams on the first,

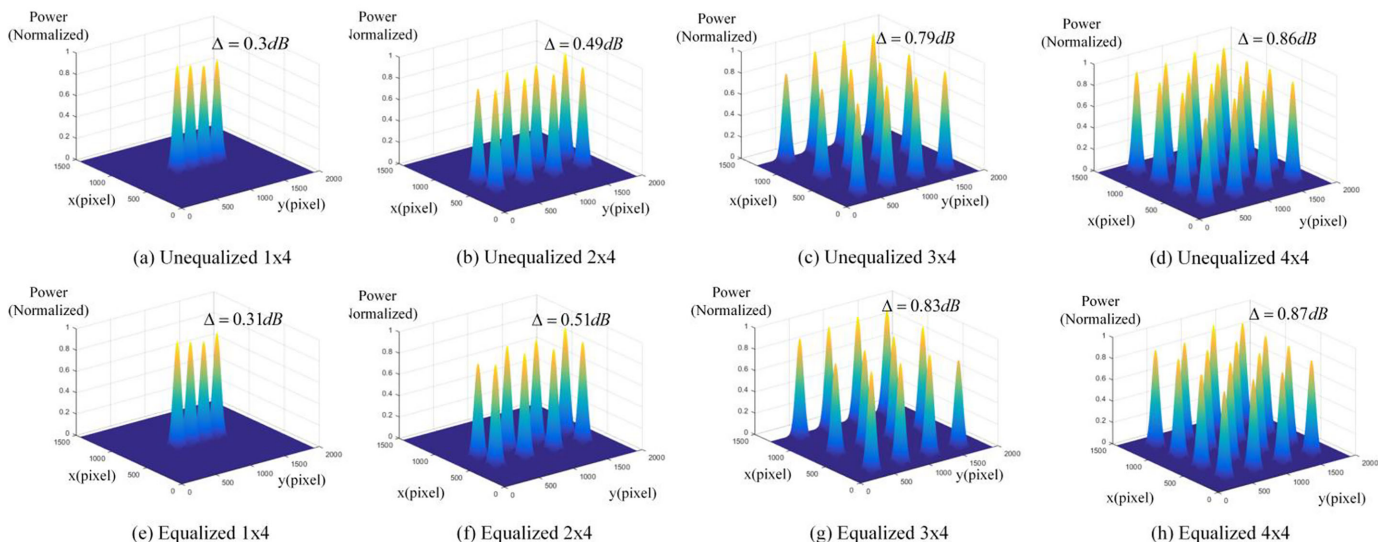


Fig. 6. Power spectral equalization in the scenario of multicast switching (1550.8 nm). (a)–(d) Unequalized power distributions, (e)–(h) Equalized power distributions.

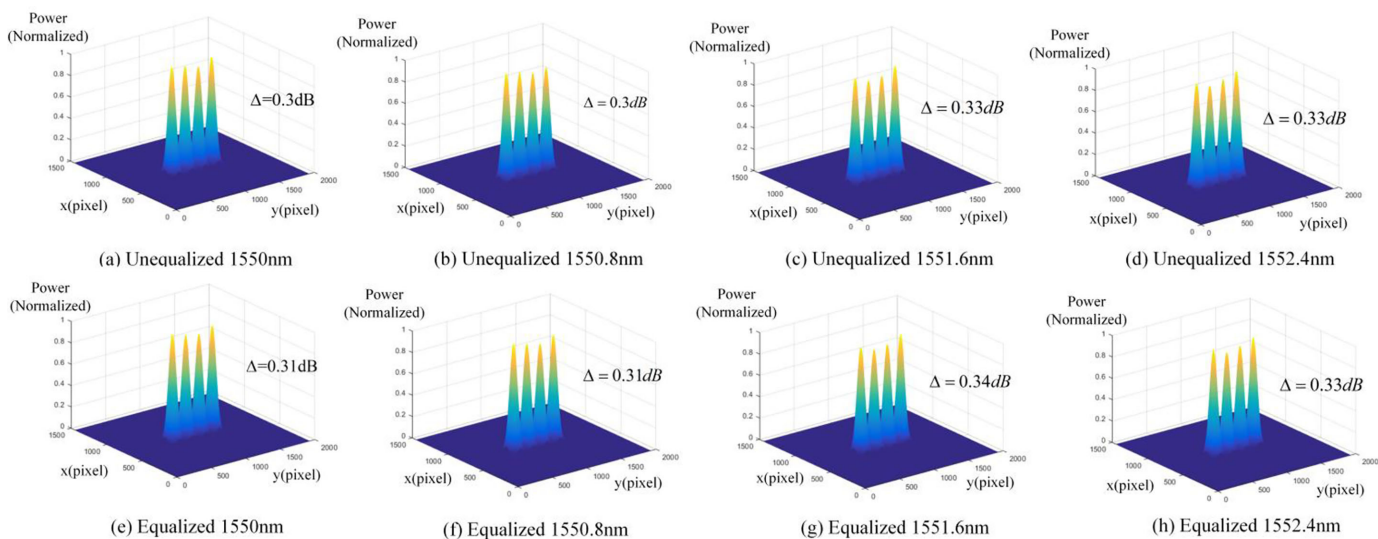


Fig. 7. Power spectral equalization of different wavelengths in the scenario of multicast switching (1×4 multicasting). (a)–(d) Unequalized power distributions, (e)–(h) Equalized power distributions.

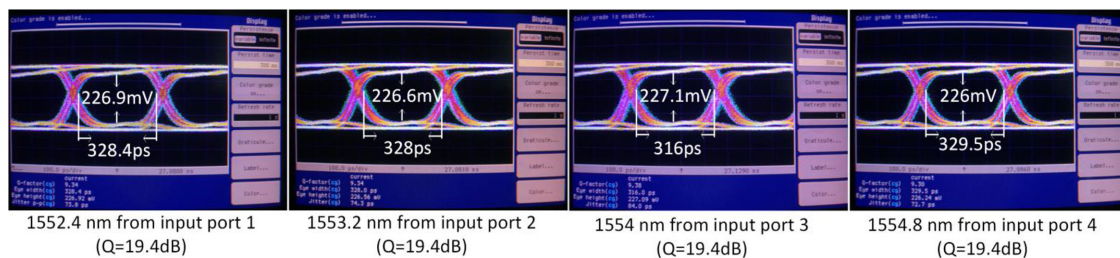


Fig. 8. Eye diagrams of four different wavelengths received at 1st output fiber port based on multicasting.

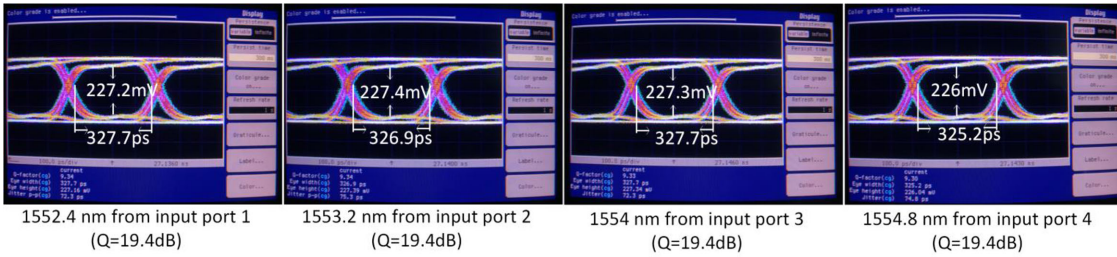


Fig. 9. Eye diagrams of four different wavelengths received at the 16th output fiber port based on multicasting.

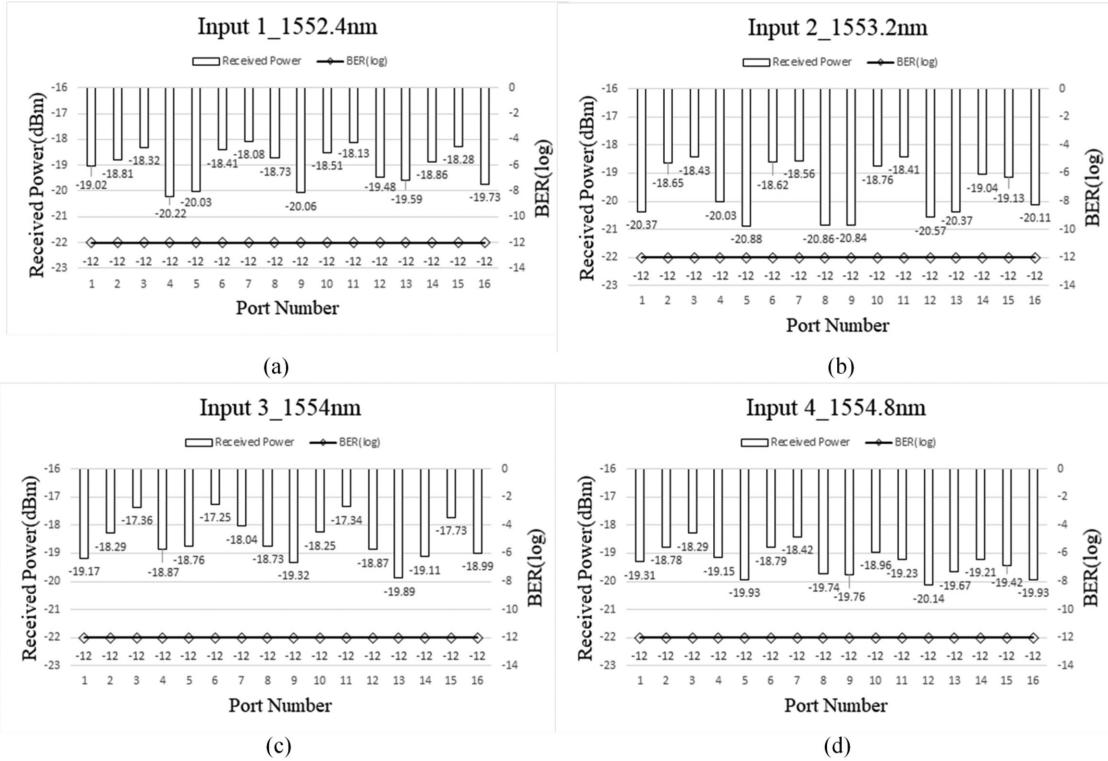


Fig. 10. Measured power & BERs in the scenarios of multicasting.

and the last output fiber port of the system. The measured Q factors are all closed to 19.4 dB, in which the estimated bit error ratios (BERs) were all less than 10^{-12} . The optical power of each wavelength launched in each input fiber port is 10 dBm. Fig. 10 shows the received optical powers of four different wavelengths at each output fiber port as a representative evaluation of experimental results delivered from the input fiber plane (port 1 ~ 4 respectively) and multicasting to 16 output fiber ports simultaneously. According to our measurement results, each optical wavelength's received power from multicasting at the output fiber plane is all in a range of $-18 \sim -20$ dBm, in which the uniformity performance is acceptable. From these experimental results of eye diagrams and received optical powers, each incident optical wavelength delivered from the input fiber plane and switched to the output fiber plane of the optical wavelength switch system in the scenario of multicasting has analyzed, and the calculated BERs from the Q factors of the

measured eye diagrams can be regarded as bit-error-free. A BER tester was also used to verify the system performance further, and the measured BERs were all the same.

IV. CONCLUSION

In this experimental research, the evaluation of a reconfigurable optical wavelength switch through the utilization of an LCoS-SLM device in an asymmetric wavelength switching architecture is reported, for the first time, in an edge node (i.e., e-ROADM) implementation. The multicasting and power spectral equalization performance was experimentally examined to achieve a digital signal transmission link speed beyond 2.5Gbps. They are important functionalities required at the edge of an optical access network. The experimental measurements have shown that the performance in terms of the uniformity of spot power distributions, crosstalk, and the BERs in multicasting scenarios

are all within an acceptable criterion. The proposed research work will offer an efficient approach for rapidly implementing an edge node to interface the optical transport network and fiber access network.

ACKNOWLEDGMENT

The authors appreciate the technical support from the Telecommunication Laboratory Chunghwa Telecom Company, Ltd., Taoyuan, Taiwan.

REFERENCES

- [1] S.-M. Lee, S.-G. Mun, M.-H. Kim, and C.-H. Lee, "Demonstration of a long-reach DWDM-PON for consolidation of metro and access networks," *J. Lightw. Technol.*, vol. 25, pp. 271–276, 2007.
- [2] G. C. Mandal, R. Mukherjee, B. Das, and A. S. Patra, "Next-generation bidirectional triple-play services using RSOA based WDM radio on free-space optics PON," *Opt. Commun.*, vol. 411, pp. 138–142, 2018.
- [3] G. C. Mandal, R. Mukherjee, B. Das, and A. S. Patra, "A full-duplex WDM hybrid fiber-wired/fiber-wireless/fiber-VLC/fiber-IVLC transmission system based on a self-injection locked quantum dash laser and a RSOA," *Opt. Commun.*, vol. 427, pp. 202–208, 2018.
- [4] A. S. Das and A. S. Patra, "Simultaneous signal transmission of different data-rates in a DWDM system employing external injection locking technique," *Opt. Laser Technol.*, vol. 64, pp. 23–27, 2014.
- [5] T. A. Strasser and J. Taylor, "ROADMS unlock the edge of the network," *IEEE Commun. Mag.*, vol. 46, no. 7, pp. 146–149, Jun. 2008.
- [6] A. Densmore *et al.*, "Compact and low power thermo-optic switch using folded silicon waveguides," *Opt. Exp.*, vol. 17, no. 13, pp. 10457–10465, 2009.
- [7] D. M. Marom *et al.*, "Wavelength-selective $1 \times k$ switches using free-space optics and MEMS micromirrors: Theory, design, and implementation," *J. Lightw. Technol.*, vol. 23, no. 4, pp. 1620–1630, 2005.
- [8] J. C. Tsai, S. T.-Y. Huang, D. Hah, and M. C. Wu, " $1 \times n^2$ wavelength selective switch with two cross-scanning one-axis analog micromirror arrays in a 4-f optical system," *J. Lightw. Technol.*, vol. 24, no. 2, pp. 897–903, 2006.
- [9] J. Kelly, "Applications of liquid crystal technology to telecommunication devices," in *Proc. Opt. Fiber Commun. Conf. Expo. Nat. Fiber Optic Eng. Conf.*, 2007, pp. 1–7.
- [10] K. Sorimoto *et al.*, "Compact and phase-error-robust multilayered AWG-based wavelength selective switch driven by a single LCOS," *Opt. Exp.*, vol. 21, no. 14, pp. 17131–17149, 2013.
- [11] D. Xie *et al.*, "LCoS-based wavelength-selective switch for future finer-grid elastic optical networks capable of all-optical wavelength conversion," *IEEE Photon. J.*, vol. 9, no. 2, Apr. 2017, Art. no. 7101212.
- [12] T. D. Wilkinson, W. A. Crossland, N. Collings, F. Zhang, and M. Fan, "Reconfigurable free-space optical cores for storage area networks," *IEEE Commun. Mag.*, vol. 43, no. 3, pp. 93–99, Mar. 2005.
- [13] P. Roorda and B. Collings, "Evolution to colorless and directionless ROADMs architectures," in *Proc. Opt. Fiber Commun. Conf./Nat. Fiber Optic Eng. Conf. OSA Tech. Dig.*, 2008, pp. 1–3.
- [14] B. Robertson *et al.*, "Demonstration of multi-casting in a 1×9 LCOS wavelength selective switch," *J. Lightw. Technol.*, vol. 32, no. 3, pp. 402–410, Feb. 2014.
- [15] T. Lu, N. Collings, B. Robertson, and D. Chu, "Design of a low-cost and compact 1×5 wavelength-selective switch for access networks," *Appl. Opt.*, vol. 54, pp. 8844–8855, 2015.
- [16] K. Yamaguchi, M. Nakajima, J. Yamaguchi, T. Hashimoto, Y. Ikuma, and K. Suzuki, "MxN wavelength selective switches using beam splitting by space light modulators," *IEEE Photon. J.*, vol. 8, 2016, Art. no. 0600809.
- [17] P. D. Colbourne, S. McLaughlin, C. Murley, S. Gaudet, and D. Burke, "Contentionless twin 8×24 WSS with low insertion loss," in *Proc. Opt. Fiber Commun. Conf. Postdeadline Papers*, 2018, Art. no. Th4A.1.
- [18] A. Rundquist, A. Efimov, and D. Reitze "Pulse shaping with the gerchberg-saxton algorithm," *J. Opt. Soc. Amer. B*, vol. 19, no. 10, pp. 2468–2478, 2002.
- [19] H.-H. Chou, C.-Y. Tsai, and C.-L. Chen, "Experimental study of reconfigurable visible light communications based on holographic spot array generations," *IEEE Photon. J.*, vol. 10, no. 2018, Art. no. 7902610.
- [20] H.-H. Chou and C.-Y. Chen, "Demonstration of asymmetric wavelength selective switch based on LCoS SLM for optical access network," in *Proc. 21st Int. Conf. Transparent Opt. Netw.*, 2019, pp. 1–5.
- [21] H. Yang, B. Robertson, P. Wilkinson, and D. Chu, "Small phase pattern 2D beam steering and a single LCOS design of 40×12 stacked wavelength selective switches," *Opt. Exp.*, vol. 24, pp. 12240–12253, 2016.
- [22] Jasper Display Corp, Product and application. [Online]. Available: <https://www.jasperdisplay.com/slm-products/>
- [23] W. Stallings, *Data and Computer Communications*. Englewood Cliffs, NJ, USA: Pearson - Prentice Hall, 2007.
- [24] Newport Corporation, Products. [Online]. Available: <https://www.newport.com/c/diffraction-gratings>
- [25] D. Wright, P. Greve, J. Fleischer, and L. Austin, "Laser beam width, divergence and beam propagation factor -and international standardization approach," *Opt. Quant. Electron.*, vol. 24, pp. S993–S1000, 1992.